A Review and Partial Reproduction of Huber et al.'s "A Novel Digital Beam-Forming Concept for Spaceborne Reflector SAR Systems"

Navi Boyalakuntla
Stanford University
pranavib@stanford.edu

Abstract— **Huber et al. propose a new digital beam-forming radar concept and a new digital signal processing approach in the paper "A Novel Digital Beam-Forming Concept for Spaceborne Reflector SAR Systems" [3]. They propose new sensor architecture in the form of a reflector and a digital feed array where historically planar phased antenna array systems were used for spaceborn SAR. They also propose a new digital signal processing technique using the signal properties of the transmitted waveform. This paper will review their contributions while providing additional background required to understand the paper following the Stanford EE 258 class. Additionally, the methodology to reproduce portions of their results is covered and discussed.**

I. Introduction

Synthetic Aperture Radar (SAR) is a type of data collection method frequently used in remote sensing. In SAR, the radar records the amount of energy reflected back after emitting a pulse to image a surface (an example being Earth) [6]. SAR simulates an antenna with a much larger aperture to produce images at higher resolutions by acquiring many data points and stitching them together to form a larger picture. This is why SAR is frequently used in remote sensing and mapping the surfaces of planets. SAR systems utilize a particular waveform where the instantaneous frequency changes linearly with time. This is also known as a chirp signal or a Linear Frequency Modulation (LFM) waveform.

Digital beam-forming is used with SAR systems to provide both a wider swath and higher resolution. Specifically, it is used for earth observation missions as it allows for a higher performance than analog beam-forming. There are many different types of digital beam-forming, including Conjugate Field Matching and SCan-On-REceive (SCORE). Huber et al. refers to these two types of digital beam-forming as Smart Multi-Aperture Radar Techniques (SMART) [3]. These SMART sensors do not require analog beam-forming and reduce hardware complexity by using digital beam-forming.

From a hardware perspective, SAR systems have historically used planar phased antenna array systems using transmit and receive modules. Due to greater loss at the swath borders, more chirps need to be sent to capture accurate data at the points where loss was higher. Parabolic reflector antennas have lower loss at the swath borders and also have high directivity. As an alternative to the phased array systems, Huber et al. propose a parabolic reflector with a digital feed array with multiple transmit and receive elements in elevation [3]. An advantage to using their proposed system is that there will be lower power demands due to the relatively light weight system.The implications of using this proposed antenna structure is that the receive aperture will be larger at the cost of needing to use a longer chirp signal.

Since the chirp signal is longer, Huber et al. propose using frequency adaptive filtering. They provided an example of the SAR system receiving information from two point scatterers where these received signals are overlapped in time. With this example, they showed that taking the Fourier transform of the overlapped region results in two distinctly different signals in the spectral domain. Then, each of these different regions can be weighted separately.

This paper reproduces the results found in this paper using concepts from the Stanford EE 258 class: Introduction to Radar Remote Sensing. This project was inspired by other attempts to reproduce Huber et al.'s work [4].

II. Additional Background Knowledge

This portion covers additional background knowledge that is helpful in understanding the Huber et al. paper.

Beamforming is a technique used to focus the radar transmitter and receiver in a particular direction. There are three types of beamforming: analog, digital, and hybrid. The technologies underpinning antenna beamforming and the different types will be discussed in this section. [8]

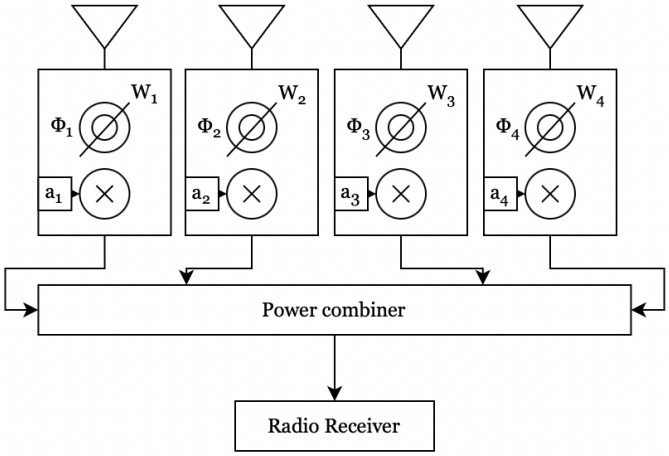

Fig. 1: An analog beam-forming receiver following Eq. 2

A. Technologies Underlying Antenna Beamforming

This section will provide an overview of several basic technologies that enable antenna beamforming.

Phased Arrays Beamforming A phased array antenna is when multiple antennas are mounted in linear arrays. It works by applying a time-delay at each antenna element which will allow the final beam to be changed with time to scan different regions of space. Additionally, analog phase shifters can be placed between before the antenna elements. These elements can actively change the phase over time which will ultimately change the antenna pattern shape.

Antenna Element Spacing The spacing between array elements is important to the final antenna RF effect. For example, quadrupling the spacing of an array from 0.5λ to 2λ will increase the main lobe gain, but also generate more sidelobes, thereby reducing the directivity. Using half-wavelength spacing is known to provide the maximum directivity [2].

Array Size The array size provides information about the gain of your antenna, which in an ideal antenna (lossless) is equal to the directivity. It follows that the gain increases by 3 dB if the number of array elements doubles following Eq. 1 [2].

$$\text{Antenna gain (db)} = \text{Element gain} + 3log_2(N) \quad (1)$$

B. Analog Beam-forming

In an analog beamforming transmitter, the baseband signal is modulated first. Then the signal is split with a power divider. The number of pathways that this power divider will divide the modulated signal into is equal to the number of antennas in the array of the transmitter. Then, the split signal has a vector of complex weights applied to it. These weights follow Eq. 2 shown below where a_k is the amplitude and ϕ_k is the phase [8]. The analog beam-forming receiver operates very similarly to the transmitter with only the power divider component being replaced with a power combiner component. Figure 1 shows an example of the layout of an analog beam-former receiver with a four antenna array [8].

$$W_k = a_k * e^{j*\phi_k} \quad (2)$$

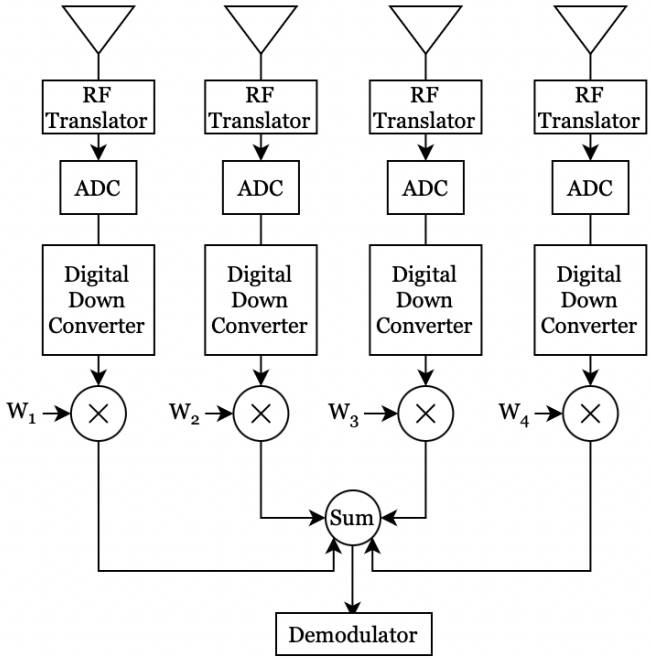

Fig. 2: A digital beam-forming receiver

C. Digital Beamforming

Digital beam-forming reduces the hardware complexity of analog beam-forming by controlling the phase and amplitude without additional hardware. Each antenna has its own RF signal and the phases and amplitude are controlled in software. Compared to analog beam-forming, digital beam-forming has more processing overhead and consumes more power. In order to transmit the signal, analog-to-digital converters (ADC) and digital-to-analog convertors (DAC) are used. All of the antennas share a local oscillator to ensure that their phases are synchronized. They all use a shared sampling clock at the ADCs and DACs for the same reason. The summation and modulation portions of the receiver and transmitter are done in software. Figure 2 shows an example of a digital beam-forming receiver [8]. In comparison

with Figure 1, all processing past the ADC is done in the digital domain which reduces hardware overhead.

III. Methodology

The steps to reproduce this paper are as follows:

1. Generate a model of the antenna system Huber et al. proposed.
2. Generate the chirp data.
3. Simulate a received chirp using the antenna parameters generated above.
4. Implement the proposed digital signal processing techniques.

A. Simulating the Antenna System

Huber et al. propose a reflector system with a parabolic reflector combined with a digital feed array of both transmit and receive elements. This antenna can be simulated in MATLAB using MATLAB's Antenna Toolbox. These feed elements are defined as perpendicular to the flight direction and facing the reflector. These different feed elements are activated dependent on the desired illumination region. The performance parameters are defined as shown in Table I in Huber et al.

There are two components needed to be designed in MATLAB: the linear feed array and the parabolic reflector. Starting with the linear feed array, the dimensions of the patch array are defined as 85 cm x 5 cm, with each individual quadratic patch being a 0.4λ patch with a spacing of 0.58λ. λ is calculated from the C-band frequency provided in Table I and is found to be $\lambda = \frac{c}{f} \approx 0.06$. The focal length defined by Eq. 3 is defined as 5.7 meters in the paper. The diameter is defined to be 10 meters. Therefore, the variable a can be found to be 0.043.

$$\text{Focal Length} = a\frac{d^2}{4} \tag{3}$$

Using all of this knowledge, an antenna can be modelled in MATLAB that looks like Figure 3. It can be seen that there is a small linear feed array on top of the antenna facing the focal plane.

The antenna pattern can be displayed using MATLAB's in-built tooling as shown in Figure 4.

B. Generating the Chirp Data

The chirp data can be generated using Eq. 4, corresponding to Eq. 13.7 in the EE 258 class notes [9]. In Eq. 4, T is the pulse length, α is the chirp rate in Hz/s, and f_c is the carrier frequency. In this case,

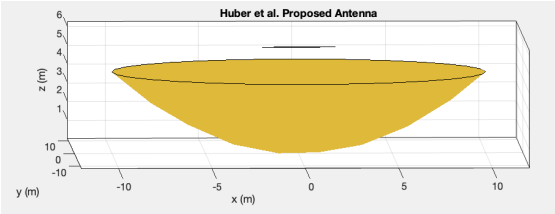

(a)

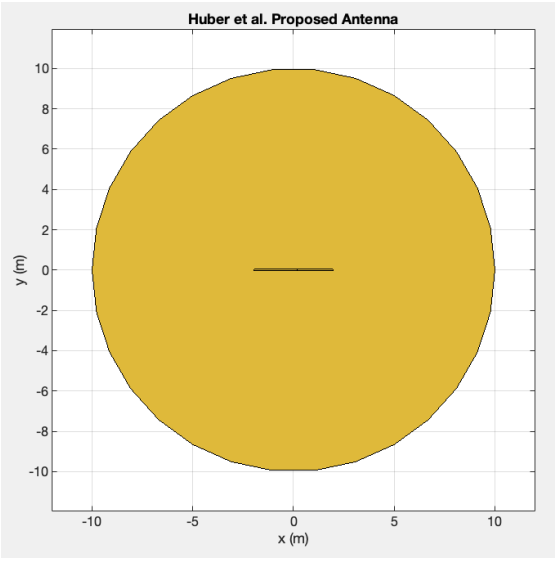

(b)

Fig. 3: Proposed parabolic antenna with linear feed array in a (a) side view and (b) top-down view

TABLE I: Reflector system performance parameters

Parameter		**Value**
Frequency	C-band	5.4 GHz
Swath Width		≥120 km
resolution (range, azimuth)	δ_{rg}, δ_{az}	≥ 8 x 8m
ambiguity-to-signal ratio	RASR, AASR	-20 dB
noise-equivalent sigma zero	NESZ	-25 dB

the carrier frequency is known to be 5.4 GHz from I. Common values for the remaining values for imaging radars could be a T of 10 ms and an α of 10^{12} Hz/s. For the purposes of this simulation, these values were adjusted to create a plot that resembled that of the paper experimentally. In Figure 4 of Huber et al. the chirp width visually is approximately between 10 MHz and 20 MHz, so these values were adjusted until that width was achieved. Following precedent set by a chirp waveform with a width around 10 MHz

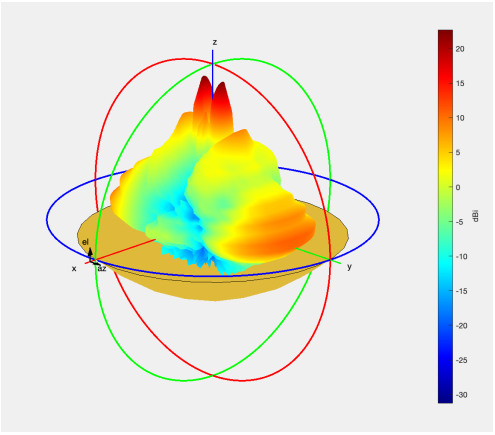

(a)

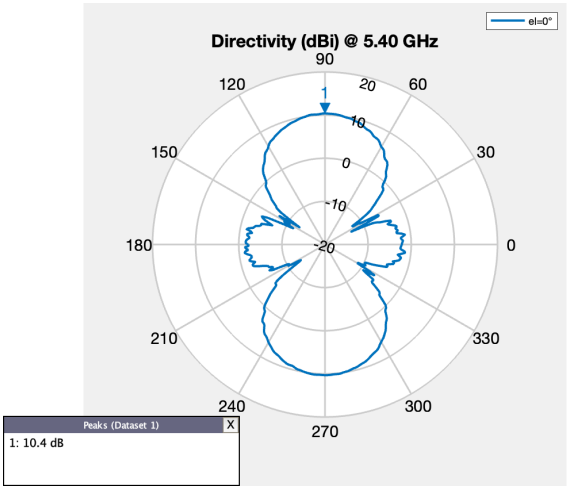

(b)

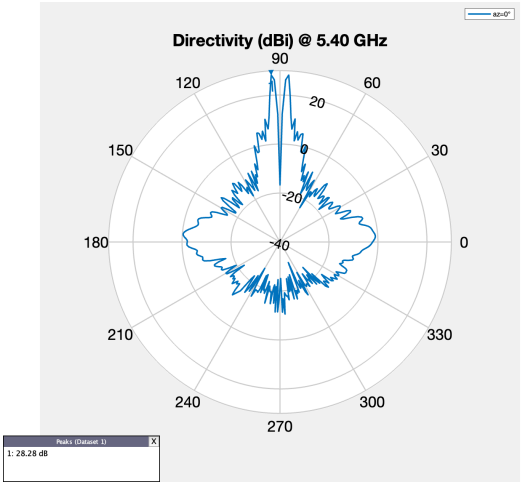

(c)

Fig. 4: Proposed antenna (a) pattern, (b) azimuth gain pattern, and (c) elevation gain pattern

in the Stanford EE 258 Radar Homework 8, a sampling frequency of 60 MHz, an α of $0.33 * 10^{12}$ Hz/s, and a T of 30 ms was used [11]. The amplitude of the transmitted signal can be assumed equal to 1 [7, p. 234].

In Figure 5, it can be seen that the chirp spectrum has a width of approximately 10 MHz and that the frequency in the spectrogram is linearly increasing.

$$s(t) = \exp\left[2\pi f_c t + 2\pi\alpha\frac{t^2}{2}\right], |t| \geq \frac{T}{2} \tag{4}$$

C. Simulation: Received Chirp Data

Using the simulated chirp and the simulated antenna information, the received chirp waveform can be calculated. Following the paper, this portion can be simulated with a point scaterrer. A flat earth is assumed following precedent in Problem 4 of the Stanford EE 258 Homework 6 [10]. Additionally, other parameters can be derived from this same source such as a velocity of 7000 m/s. From Stanford EE 258 Homework 6 Problem 1, a pulse repetition frequency of 20 Hz is extracted for this imaging radar [10]. This algorithm to simulate the received signal using the antenna parameters generated in MATLAB follows *Digital Signal Processing Techniques and Applications in Radar Image Processing* written by Dr. Bu-chin Wang [4] [7].

It can be assumed that the antenna length, L, is 1 meter following parameters set on p. 233 of Wang, Bu-Chin [7]. To find the number of azimuth samples for the algorithm, Eq 8 is used, where L_s is equal to the synthetic aperture length and A_s is equal to the azimuth sample spacing [7, p. 234]. A_s is shown in Eq. 7. Synthetic aperture length is defined by Eq. 6 where R_0 is the closest range of the target and θ_H is the radar 3-dB beam-width as defined in Eq. 5 [7, p. 234]. R_0 can be assumed to be 200 km as planetary imaging satellites perform better in the LEO range [1].

$$\theta_H = \frac{\lambda}{L} \tag{5}$$

$$L_s = R_0\theta_H \tag{6}$$

$$A_s = \frac{V}{f_{PRF}} \tag{7}$$

$$\text{Number of Azimuth Samples} = \text{int}(\frac{L_s}{A_s}) \tag{8}$$

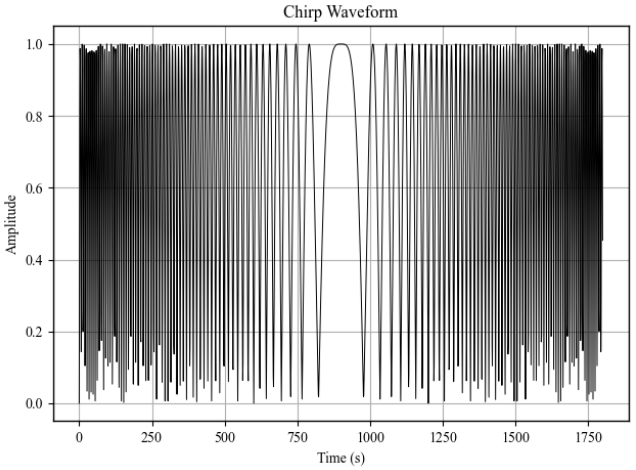

(a)

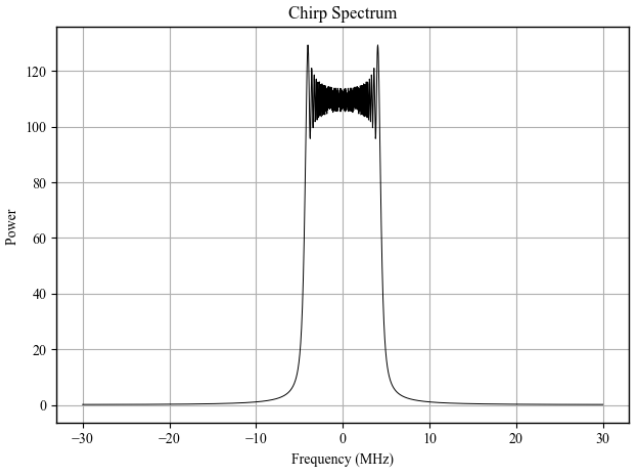

(b)

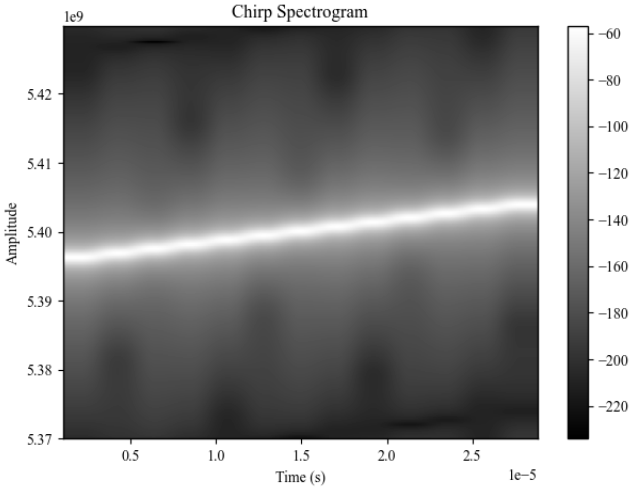

(c)

Fig. 5: Simulated chirp waveform (a) in time, (b) in frequency, and (c) the chirp spectrogram

An assumption being made to simplify this simulation is that the slant range different is less than a quarter of the range resolution allowing range migration correction to not be required [7, p. 234]. The reflection coefficient is also assumed to be 1 [7, p. 234]. The baseband signal returned from the point reflector, or received baseband, is expressed as Eq. 9, where τ_{u_i} is the echo delay time for a target located at (R_0, y_1) with the radar at position (0, u_i) [7, Eq. 8.5a] [7, Eq. 8.5b].

$$r_b(u_i, t_n) = \exp\left[-j2\pi f_c \tau_{u_i} + j\pi\alpha(t_n - \tau_{u_i})\right] \tag{9}$$

The echo delay time τ_{u_i} can be expressed as Eq. 10.

$$\tau_{u_i} = \frac{2\sqrt{(u_i - y_1)^2 + R_0^2}}{c} \tag{10}$$

For this simulation, the number of azimuth samples was found to be equal to 31,725 based on the assumed parameters. Techniques discussed in Chapter 13 of the Stanford EE 258 class notes and Wang, Bu-chin to find the received baseband signal can be used [9, pp. 315-350] [7]. Specifically, pages 340 to 349 in the Stanford EE 258 class notes provide instruction for how to implement an end-to-end SAR processor. Figure 6 shows the received baseband in time, frequency, and its spectrogram. It can be noted that the main difference is a frequency shift visibly seen in Figure 6b with the shift of the chirp spectrum to the right.

As described in Section 5 of Huber et al., the input to the digital beam former is an N-dimensional raw data vector, $\mathbf{u}^T(t)$. Huber et al. describes the received signal as the transmitted waveform, $s(t)$, weighted with the individual complex channel pattern determined by the antenna $\mathbf{g}^T(\theta)$ with thermal receiver noise $\mathbf{n}^T(t)$. To factor in the antenna effects, the antenna gain at each angle can be found using MATLAB.

The steps taken to simulate the received baseband signal with the antenna specific effects factored in are listed in detail below:

1. Calculate the number of azimuth samples using Eq. 8.
2. Determine the list of azimuth samples using the azimuth sample spacing from Eq. 7 and the number of azimuth samples from Eq. 8. This list of azimuth samples is equal to the vector of u values to will be used to calculate the rest of the information.

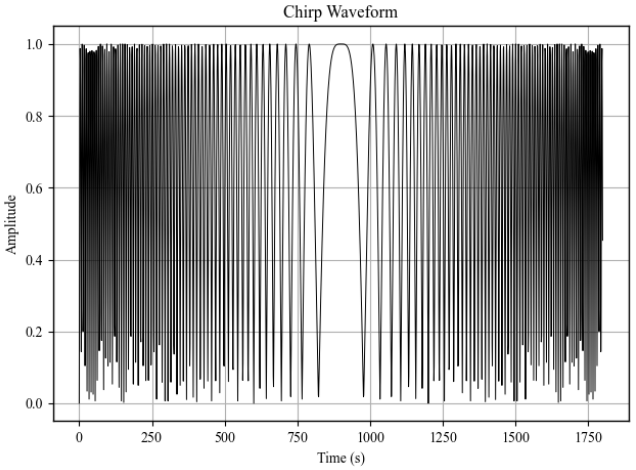

(a)

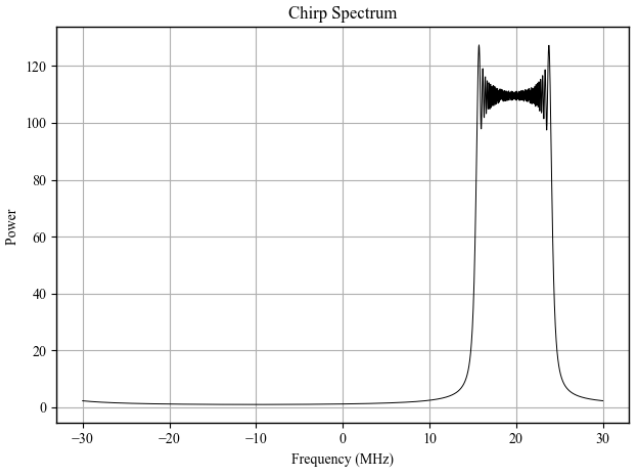

(b)

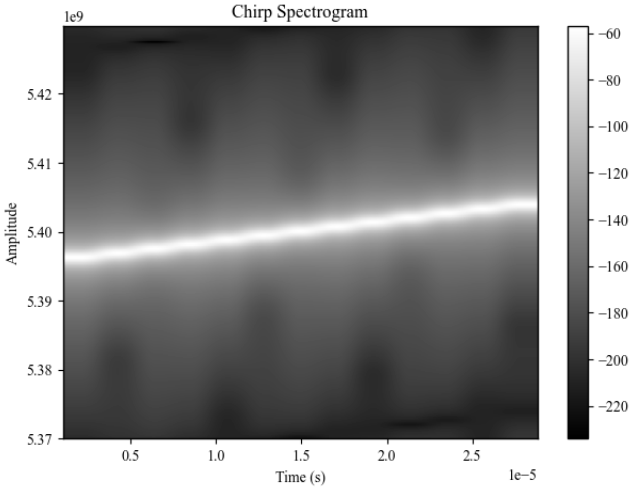

(c)

Fig. 6: Simulated received baseband waveform (a) in time, (b) in frequency, and (c) its spectrogram

3. Calculate the following for each azimuth sample (u_i) as described on page 234 of *Digital Signal Processing Techniques and Applications in Radar Image Processing*:
   (a) Calculate τ_{u_i} using Eq. 10.
   (b) Calculate the received baseband signal using Eq. 9.
4. The next step in this process is to factor in the antenna effects.
   (a) Store the antenna gain at each angle value.
   (b) Convert these angle values to azimuth values. If the azimuth spacing is smaller than the spacing between the angle values that MATLAB has generated, average the nearest gains to compute the gain at the desired azimuth. To factor in the effects of the antenna, the gain can be convolved with the received baseband signal at each u_i .
   (c) At this point, the thermal noise from the receiver needs to be added in. This noise can be randomly generated, but must be proportional to the receiver bandwidth [3]. Figure 7 shows the final simulated received baseband waveform. The most noticeable change is the addition of noise in the chirp spectrum and chirp waveform. The chirp spectrogram has not changed much at this point.

Figure 8 visualizes the antenna effects on the received baseband waveform before and after noise is added [3] The effect is slightly less visible after the noise is added, but after closer inspection can be found at the edges.

D. Proposed Digital Signal Processing Techniques

In the paper, four seperate digital beam forming algorithms are covered.

1. Basic unity weighting beam former
2. Conjugate Field Matching (CFM) without further processing
3. Range compression + CFM: Independent from the pulse length and performs optimally
   (a) Range compress the individual data stream before beam forming.
   (b) Combine the raw data from the activated channels using CFM.
4. Blocked adaptive beam former
   (a) Raw data blocks of 256 samples are range compressed.
   (b) Combine these streams with CFM.

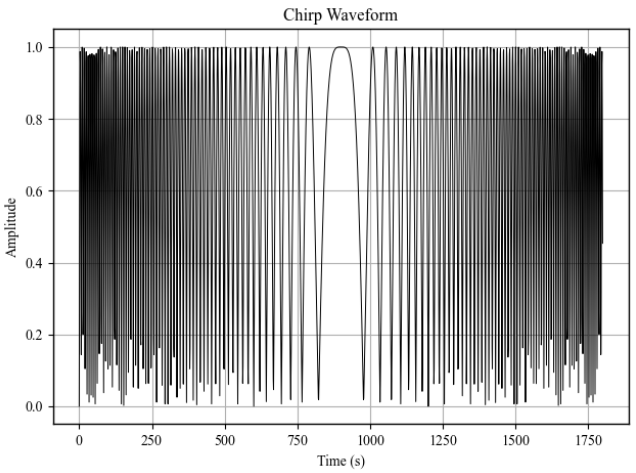

(a)

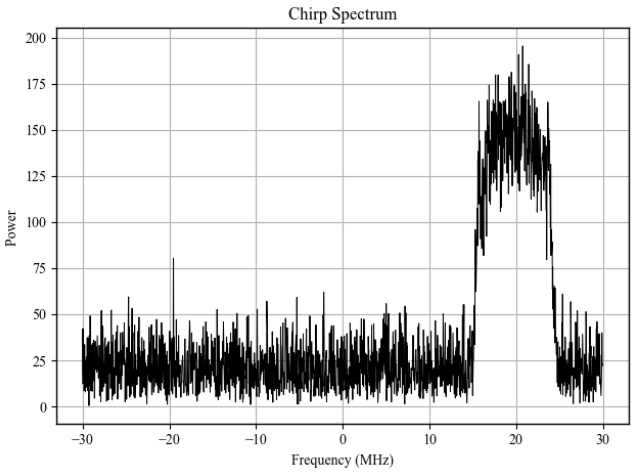

(b)

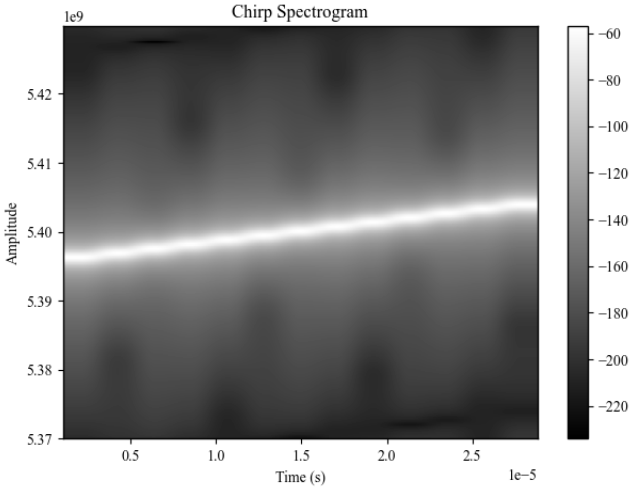

(c)

Fig. 7: Simulated received baseband waveform after antenna effects and noise are considered (a) in time, (b) in frequency, and (c) its spectrogram

The first three algorithms are not novel and serve as a comparison for the fourth algorithm. The advantage to using the blocked adaptive beam former is the lighter hardware requirements due to the filter only requiring 256 coefficients (FIR filter). In the third algorithm, since the signal would not be blocked and processes, a filter with many thousands of coefficients would be required (closer to an IIR filter). Equation 11 determines the weights to apply to the channel with the CFM algorithm.

$$\mathbf{w}^T(k) = \frac{g*(k)}{g^T(k)g*(k)} \tag{11}$$

The fourth algorithm is provided in the context of when, for example, the received baseband signals from two point reflectors overlap in the time domain. Huber et al. propose taking the FFT to separate out the overlapped region into two distinct chirp signals in the frequency domain. They then propose implementing a block-based frequency-domain adaptive filtering algorithm to process both of the unique frequency components. They do not provide much more information on how to implement this. Below I have detailed a hypothetical implementation for a frequency-based adaptive LMS algorithm for this use case [5]. This LMS algorithm can update the weights for different chirp signals weighted with different feed element patterns.

1. Given the original overlapped signal and a reference signal (in the frequency domain), divide the signal up into 256-length blocks. In a real-time system, store the 256 samples in a buffer and process as needed.
2. Since the proposed FIR filter length is 256, the entire block size will be the window. Therefore, invert the order of the reference signal block to then take the dot product with a filter coefficient vector. This filter coefficient vector will be set to some initial values (potentially 0).
3. An error value can be calculated by subtracting this dot product from the original overlapped signal.
4. Then, the filter coefficients can be updated by adding a scaled version of the error value multiplied by the inverted reference signal.
5. After enough iterations, the filter will stabilize and the radar data can be processing with a lower hardware overhead for multiple frequencies overlapping.
6. If this is done in a real-time system, portions of the previous blocks will have to be stored.

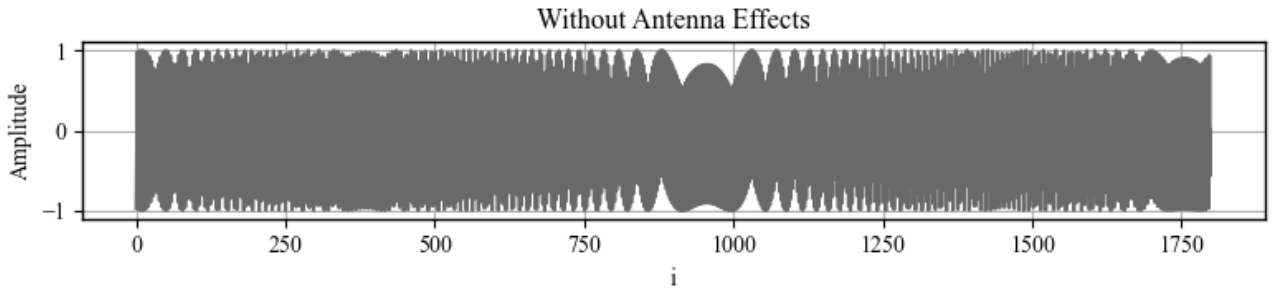

(a)

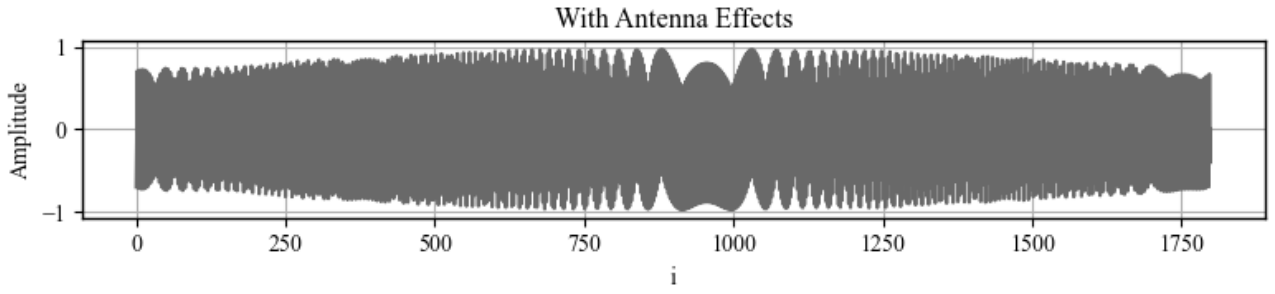

(b)

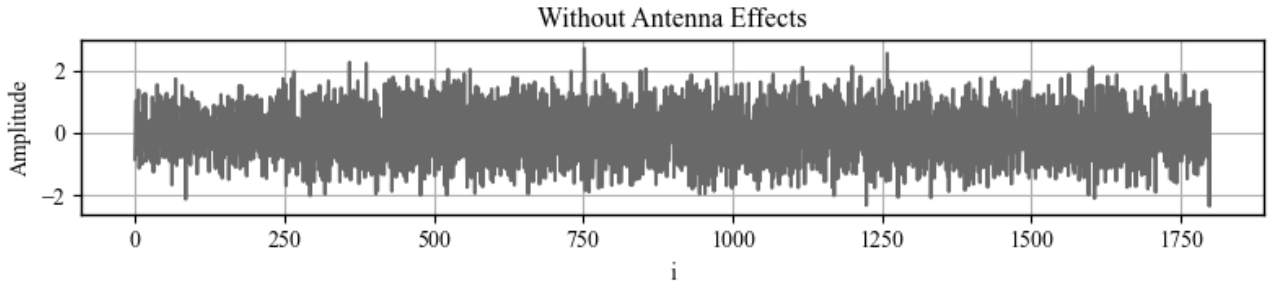

(c)

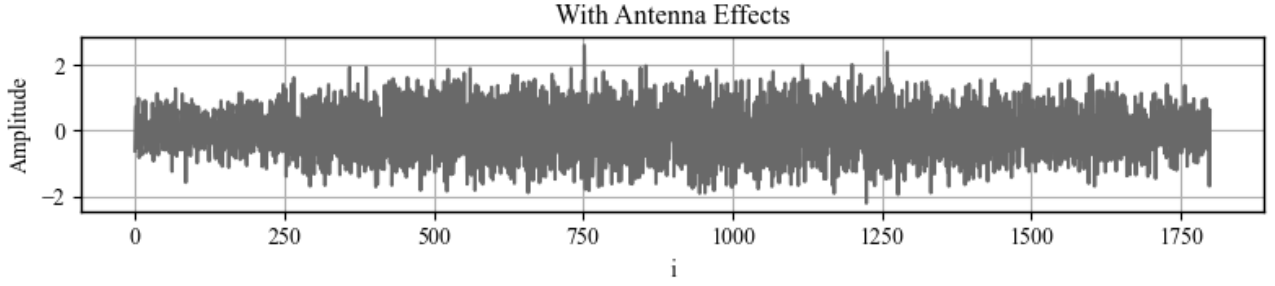

(d)

Fig. 8: Simulated received baseband waveform (a) without antenna effects, (b) with antenna effects, (c) with noise/without antenna effects, and (d) with noise/with antenna effects

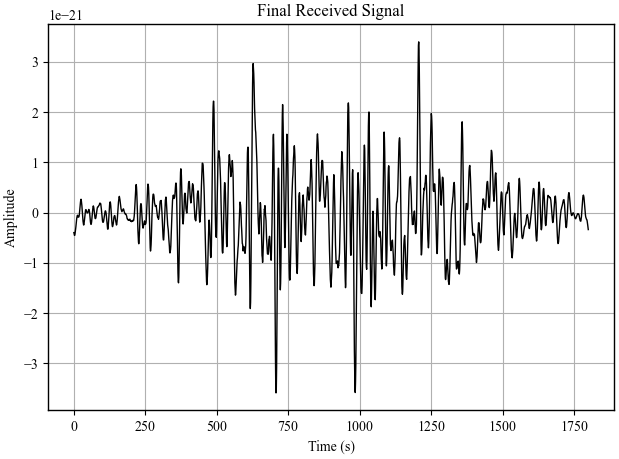

Fig. 9: Time domain signal of the signal reflected from the point scatterer

IV. Results

To calculate results from the point scatterers, two scenarios were considered. The first scenario is with a point scatterer, following the methodology section. The second scenario is when two point scatterer observed under different aspect angles are received at the same time and have an overlapping region in the time domain.

With the first scenario, the first step to receiving the data is to apply range compression. Chirp signals can be compressed by using a matched filter which involves convolving the chirp waveform with its complex conjugate [9]. Now, the CFM algorithm for the weights can be implemented using Eq. 11. In Figure 10, the amplitude of the chirp spectrum has decreased significantly due to CFM algorithm. Additionally, this signal can be confirmed to still be a chirp signal via the linearly increasing frequency in the spectrogram.

Upon visual inspection of Figure 9, there is a peak just before time at 1250 seconds alluding to that potentially being the point reflector. Further work to attenuate noise with a filter can be implemented along with further efforts to optimize the chirp signal. Additionally, the amplitude is very small for all of these peaks after the CFM algorithm has been implemented.

Due to limitations in time, the frequency-adaptive filtering algorithm has not yet been implemented. However, Figure 11 replicates Figure 4 in Huber et al. [3]. This figure was produced by taking the Fourier transform of the overlapped region of two chirp signals in time which yielded two distinct chirp signals

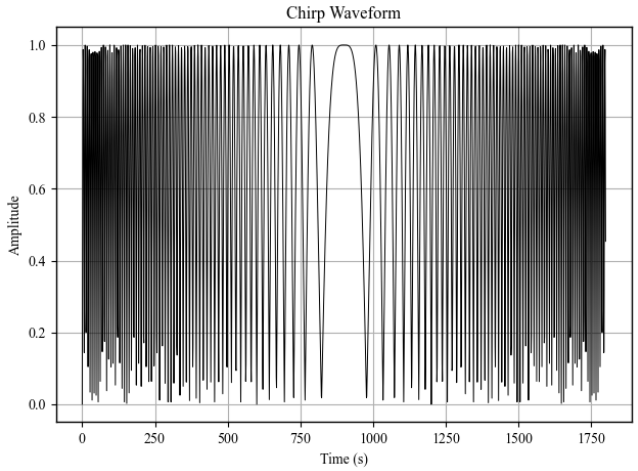

(a)

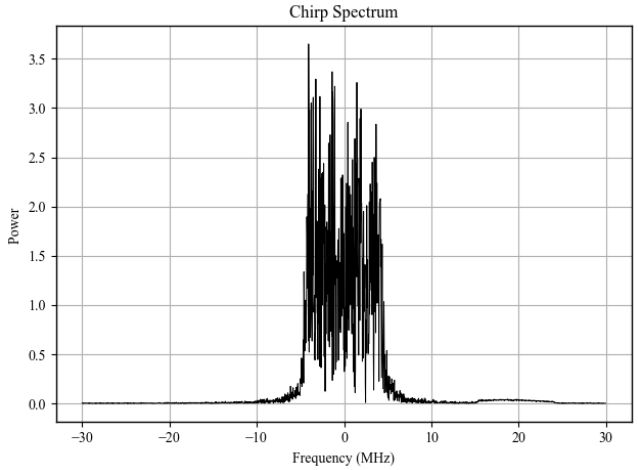

(b)

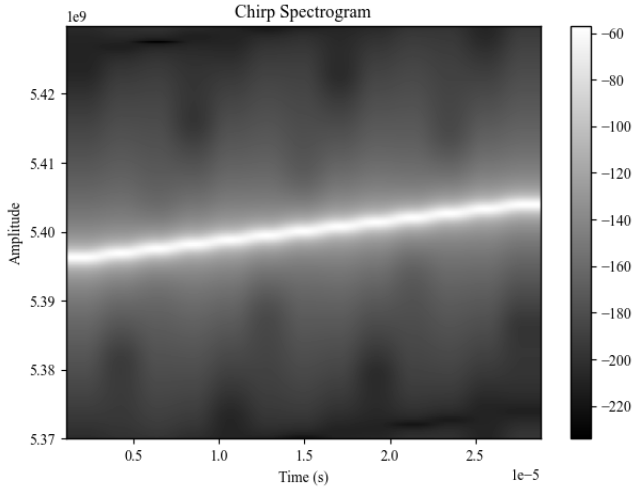

(c)

Fig. 10: Received chirp signal after range compression and CFM (a) in time, (b) in frequency, and (c) its spectrogram

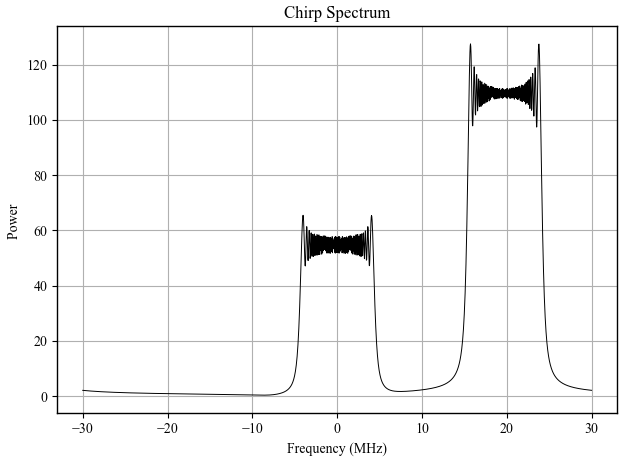

Fig. 11: Chirp spectrum of the overlapped region

in frequency.

V. Conclusion

Huber et al. presents a new digital beamforming technique using frequency adaptive filtering along with a new unfoldable reflector antenna. This paper attempts to reproduce some of the work proposed in the paper with the goal of describing the steps in detail for further work and reproduction. As noted in Section IV above, further work on improving the chirp parameters along with noise attenuation is necessary to gain a clear peak for the point reflector.

Further work to model this radar signal with more point scatterers or different types of scatters would further confirm the results of this paper [3] Additionally, simulating the proposed antenna against a more traditional planar array antenna with a model not assuming a flat earth would provide a more accurate simulation.

References

[1] European Space Agency. Esa - types of orbits.

[2] Dr. Mohamed Nadder Hamdy. Beamformers explained.

[3] Sigurd Huber, Marwan Younis, Anton Patyuchenko, and Gerhard Krieger. A novel digital beam-forming concept for spaceborne reflector sar systems. pages 238–241, 2009.

[4] Rishi Kakade. Digital beam forming for spaceborne reflector sar.

[5] J.C. Lee, C.K. Un, and D.H. Cho. A frequency-weighted block lms algorithm and its application to speech processing. *Proceedings of the IEEE*, 73(6):1137–1138, 1985.

[6] Franz Meyer. Spaceborne synthetic aperture radar: Principles, data access, and basic processing techniques.

[7] Bu-Chin Wang. *Digital Signal Processing Techniques and Applications in Radar Image Processing*.

[8] RF Wireless World. Analog beamforming vs digital beamforming — difference between analog beamforming and digital beamforming.

[9] Howard Zebker and Dustin Schroeder. Ee 258 notes.

[10] Howard Zebker and Dustin Schroeder. Stanford ee 258 homework 6.

[11] Howard Zebker and Dustin Schroeder. Stanford ee 258 homework 8.